Direct numerical simulations of particle-laden isotropic turbulence. Pseudo-spectral solver

Michał Rajek*

Institute of Fluid-Flow Machinery, Polish Academy of Sciences
14 Fiszera Street, 80-231 Gdansk, Poland

Abstract

In this work an in-house pseudo-spectral direct numerical simulations solver for particle-laden forced isotropic turbulence is developed. The code has been validated against the results of a decaying three-dimensional Taylor-Green vortex field at moderate Reynolds number. The solver can be relatively easily adapted for large-eddy simulations using the concept of spectral eddy-viscosity. The solver is coupled with the Lagrangian particle tracking of a dispersed phase essentially approximated by point-particles whose particle-to-fluid density ratio is $\mathcal{O}(10^3)$. High order Lagrange interpolation and combined implicit-explicit time-integration scheme are used to solve the particle equation of motion.

Keywords: pseudo-spectral; DNS; isotropic turbulence; inertial particles

1 Introduction

Turbulent dispersed multiphase flows are inherent part of many environmental and industrial processes. Among many others, this includes sand and dust storms, rain formation, sedimentation processes, cyclone separation, pharmaceutical sprays, fuel atomization and spray combustion. Obviously, an in-depth understanding of suspended particle dynamics in turbulent flows is of significant importance for further developments in the foregoing areas. Due to inevitable particle-turbulence and particle-particle interactions, possibly coupled with the heat-transfer, evaporation, or even chemical reactions, particle-laden turbulent flows are usually associated with multi-scale (or even multi-physics) complex phenomena yet to be fully understood, accurately predicted, and most importantly, controlled in order to obtain a desired change in the flow behavior. Due to a wide range of spatial and temporal scales, experimental investigations of dispersed turbulent multiphase flows often become problematic (or even unfeasible). On the other hand, it should be noted that both the continuous improvement of numerical methods and the rapid growth of computing capabilities provide a unique opportunity to study these complex flows. For a comprehensive review of recent advancements in the numerical simulation of particle-laden turbulent flows, the reader can refer to [1, 2].

Insofar as the physics underlying particle-laden flows is concerned, one should confine to the simplest examples of turbulent flows, usually associated with simple geometries. This includes for example the flow through a channel, past a sphere or a flat plate.

*Corresponding Author. Email address: mrajek@imp.gda.pl
https://doi.org/10.58139/c82v-cy47

Some assumptions can also be made regarding the dispersed phase. In the case of dilute suspensions of small particles, when compared to the smallest length scales of a turbulent flow, dispersed entities can usually be approximated by point-particles. The Lagrangian tracking of such individual mass-points can be effectively coupled with the Eulerian direct numerical simulations of the continuous carrier phase, essentially leading to the so-called point-particle direct numerical simulations.

In this work, the author restricts his attention to homogeneous isotropic turbulence which is considered as the most fundamental turbulent flow. In addition to that, isotropic turbulence can be realized (to some extent) experimentally [3]. The reader is also briefly acquainted with some key important elements of the pseudo-spectral solver developed for the purpose of studying suspended particle dynamics in homogeneous and isotropic turbulence.

2 The equations of fluid motion in Fourier space

In the case of an incompressible fluid, the continuity equation acquires the form of

$$\frac{\partial U_\alpha(\boldsymbol{x},t)}{\partial x_\alpha} = 0, \tag{1}$$

where $U_\alpha(\boldsymbol{x},t)$ is the fluid velocity at position $\boldsymbol{x}$ and time t. The conservation of momentum is governed by the Navier-Stokes equation in the form of

$$\frac{\partial U_\alpha}{\partial t} + U_\beta \frac{\partial U_\alpha}{\partial x_\beta} = -\frac{1}{\rho}\frac{\partial P}{\partial x_\alpha} + \nu\nabla^2 U_\alpha + F_\alpha, \tag{2}$$

where P is the pressure field, F is a body force, and ν is the kinematic viscosity of the fluid. For the sake of simplicity, the explicit dependence on both the position and time is dropped. According to the Reynolds decomposition [4], an arbitrary velocity field can be decomposed into the ensemble mean and a fluctuation about that mean leading to

$$U_\alpha = \langle U_\alpha \rangle + u_\alpha. \tag{3}$$

The flow can only be isotropic in the absence of preferential directions. This essentially implies the mean velocity is either zero or constant. In this work, the author confines his attention to turbulent flows for which

$$\langle U_\alpha \rangle = 0. \tag{4}$$

In fact, the above condition is often referred to as the zero-mean-flow condition. With the substitution of Eq. (3), and the use of Eq. (4), the equation governing the fluid motion, Eq. (2), can be rewritten to obtain

$$\frac{\partial u_\alpha}{\partial t} + u_\beta \frac{\partial u_\alpha}{\partial x_\beta} = -\frac{1}{\rho}\frac{\partial p}{\partial x_\alpha} + \nu\nabla^2 u_\alpha + f_\alpha, \tag{5}$$

which essentially describes the evolution of velocity fluctuations. In addition to Eq. (4), the velocity field (or the computational box, strictly speaking) must also be infinite in extent. In practice, the fluid is confined to a cubic box of side L_B, with periodic boundary conditions additionally imposed on its sides [5]. In this case, the velocity field can be

expanded in a Fourier series according to

$$u_\alpha(\boldsymbol{x},t) = \left(\frac{2\pi}{L_B}\right)^3 \sum_{\boldsymbol{k}} \hat{u}_\alpha(\boldsymbol{k},t) e^{i\boldsymbol{k}\cdot\boldsymbol{x}} = \left(\frac{2\pi}{L_B}\right)^3 \sum_{\boldsymbol{k}} \hat{u}_\alpha e^{i\boldsymbol{k}\cdot\boldsymbol{x}}, \tag{6}$$

where $(\hat{})$ is used to distinguish the Fourier-transformed variables from their physical space counterparts; $\boldsymbol{k} = k_0\boldsymbol{n} = k_0(n_1\boldsymbol{e_1} + n_2\boldsymbol{e_2} + n_3\boldsymbol{e_3})$ is the wavevector with $k_0 = 2\pi L_B^{-1}$ being the lowest non-zero wavenumber; n_i are integers. In the case of $L_B \to \infty$, the Fourier transform, Eq. (6), takes the following integral form

$$u_\alpha = \int \mathrm{d}^3\boldsymbol{k}\ \hat{u}_\alpha e^{i\boldsymbol{k}\cdot\boldsymbol{x}}, \tag{7}$$

and

$$\hat{u}_\alpha = (2\pi)^{-3} \int \mathrm{d}^3\boldsymbol{x}\ u_\alpha e^{-i\boldsymbol{k}\cdot\boldsymbol{x}}. \tag{8}$$

In should noted that in the Fourier space the differential operator $\partial/\partial_{x_\alpha}$ is reduced to a simple complex multiplier ik_α. Taking advantage of this property, the continuity equation in the Fourier space becomes

$$ik_\alpha \hat{u}_\alpha = 0, \tag{9}$$

whereas with some minor rearrangement, the Navier-Stokes equation, Eq. (5), takes the form of

$$\frac{\partial \hat{u}_\alpha}{\partial t} + ik_\beta \mathcal{F}\left(u_\alpha u_\beta\right) = -ik_\alpha \frac{\hat{p}}{\rho} - \nu k^2 \hat{u}_\alpha + \hat{f}_\alpha, \tag{10}$$

where $\mathcal{F}$ denotes the Fourier transform, and $k^2 = k_\alpha k_\alpha = |\boldsymbol{k}|^2$. The pressure term on the right-hand side can be eliminated with the use of Eq. (9), eventually leading to

$$\left(\frac{\partial}{\partial t} + \nu k^2\right) \hat{u}_\alpha = -ik_\gamma P_{\alpha\beta}(\boldsymbol{k}) \mathcal{F}\left(u_\beta u_\gamma\right), \tag{11}$$

where $P_{\alpha\beta}(\boldsymbol{k}) = \delta_{\alpha\beta} - k_\alpha k_\beta / k^2$ is the projection tensor. Using the convolution theorem, the non-linear term can be evaluated by summing the Fourier coefficients leading to

$$\mathcal{F}(u_\beta u_\gamma) = \left(\frac{2\pi}{L_B}\right)^3 \sum_{\boldsymbol{p}+\boldsymbol{q}=\boldsymbol{k}} \hat{u}_\beta(\boldsymbol{p}) \hat{u}_\gamma(\boldsymbol{q}). \tag{12}$$

However, this requires $\mathcal{O}(N^2)$ operations where N is the number of nodes in each spatial direction. Obviously, the computational cost associated with the evaluation of Eq. (12) can become prohibitively large.

3 Pseudo-spectral approximation

Consider the velocity field $u_\alpha(\boldsymbol{x})$ defined on points of the discrete $N \times N \times N$ grid such that $x_\alpha = nL_B/N$ for $n = 0, 1, ..., N-1$, and whose Fourier coefficients $\hat{u}_\alpha(\boldsymbol{k})$ are defined for any $\boldsymbol{k}$ essentially satisfying $-N/2 + 1 \leq k_\alpha \leq N/2$. The velocity field is confined to a cubic box of side $L_B = 2\pi$, where periodic boundary conditions are imposed so that

$$u_\alpha(x_1 + 2\pi n_1, x_2 + 2\pi n_2, x_3 + 2\pi n_3) = u_\alpha(x_1, x_2, x_3, t), \tag{13}$$

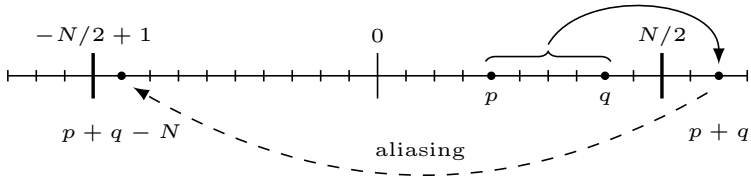

Figure 1: Aliasing errors arising from the application of the discrete Fourier transform.

where n_1, n_2, n_3 are integers. In this case, the velocity field (and the pressure field, obviously) can be expanded in the Fourier series according to Eq. (6). For completeness, the maximum resolved wavenumber in each spatial direction is $k_{\max} = k_0 N/2 = N/2$. Taking advantage of the convolution theorem, Eq. (12), Orszag [6] put forward the so-called pseudo-spectral approximation in which the non-linear term is first evaluated in the physical space, and then transformed back to the Fourier space. Using the Cooley & Tukey algorithm [7], often referred to as the Fast Fourier Transform (FFT) algorithm, the non-linear term can be evaluated in $\mathcal{O}(N\log N)$ operations. However, this comes at a price. The use of the discrete Fourier transform introduces the so-called aliasing errors, see Fig. 1, which should be removed in order to obtain reliable and stable numerical simulations. These errors are most often removed using the so-called "2/3" rule. In this method, the discrete Fourier transform is evaluated using M rather N points, where $M \geq 3/2N$. To get a more detailed description of this approach, the reader can refer to [8]. Patterson & Orszag [9] indicated that if the Fourier coefficients are truncated according to $|\boldsymbol{k}| \leq \sqrt{2}N/3$, then the aliasing errors are significantly reduced. The very same authors reported that the remaining part of the aliasing errors can be effectively removed if the convolution sum, Eq. (12), is evaluated at two grids shifted by half a grid cell in each direction, and subsequently averaged. In this work, the author removes the aliasing errors using the combined approach proposed by Patterson & Orszag. This dealiasing scheme, although being less efficient than the "2/3" rule, allows to retain more Fourier modes and thus becomes a method of choice when memory is a concern.

Due to numerical stability [10], the Navier-Stokes equation, Eq. (5), is often expressed in the rotation form which can be transformed to the Fourier space according to

$$\left(\frac{\partial}{\partial t} + \nu k^2\right) \hat{u}_\alpha = P_{\alpha\beta}\mathcal{F}(\boldsymbol{u} \times \boldsymbol{\omega})_\beta + \hat{f}_\alpha, \tag{14}$$

where $\boldsymbol{\omega}$ is the vorticity field in the physical space, and $\hat{f}_\alpha$ is an artificial forcing used to sustain turbulence.

In this work, the author uses a deterministic forcing similar to that introduced in [11] and [12], i.e.,

$$\hat{f}_\alpha(\boldsymbol{k}) = \begin{cases} (\epsilon_f/2E_f)u_\alpha(\boldsymbol{k}) & 0 < k < k_f \\ 0 & \text{otherwise,} \end{cases} \tag{15}$$

where ϵ_f is the energy injection rate, E_f is the total kinetic energy contained in the forced wavenumber band, and k_f is the maximum forced wavenumber, usually not exceeding $2\sqrt{2}$. The forcing has to be adjusted so that both the smallest, dissipative scales, and the largest, energy containing scales are accurately resolved on a finite grid.

4 Time integration of the Navier-Stokes equations

Stable and accurate integration of the equations governing the fluid motion requires the spatial and temporal discretization errors to be kept at a relatively low level. According to the best of the author's knowledge, the viscous term in the Navier-Stokes equation is usually integrated implicitly using the integrating factor technique [13, 14], wheres the explicit second-order (also third- and fourth-order) Runge-Kutta [15, 16] or second-order Adams-Bashforth [17] methods are employed to advance the convective term in time. Some authors also combined the implicit Crank-Nicolson and second-order Adams-Bashforth methods for viscous and convective term, respectively [18].

Introducing a time step, such that $t_n = n\Delta t$, the velocity field can be advanced in time according to

$$\hat{u}_\alpha^{n+1} = \hat{u}_\alpha^n e^{-\nu k^2 \Delta t} + \frac{\Delta t}{24}\Big[55\Pi^n e^{-\nu k^2 \Delta t} - 59\Pi^{n-1} e^{-2\nu k^2 \Delta t} + 37\Pi^{n-2} e^{-3\nu k^2 \Delta t} - 9\Pi^{n-3} e^{-4\nu k^2 \Delta t}\Big], \tag{16}$$

where

$$\Pi^n = P_{\alpha\beta}\hat{N}_\beta^n + \hat{f}_\alpha^n. \tag{17}$$

It should be noted that the forcing term, $\hat{f}_\alpha$, is in general designed to be solenoidal and statistically isotropic, and thus can be safely added to the non-linear term before the projection tensor is applied leading to

$$\Pi^n = P_{\alpha\beta}(\hat{N}_\beta^n + \hat{f}_\beta^n). \tag{18}$$

In fact, this minor modification corrects the round-off errors resulting from the repeated evaluation of the discrete Fourier transforms, thus allowing long-term time-integration of the Navier-Stokes equation. The foregoing scheme, essentially composed of the integrating factor technique and the fourth-order Adams-Bashforth methods, seems to constitute a reasonable trade-off between accuracy and the computational cost of the simulation.

5 Preliminary results

In this section some results are compared against the reference data reported in [19] for a three-dimensional, incompressible Taylor-Green vortex at $Re = 1600$. This vortex field essentially develops from a single-mode initial condition defined according to

$$\begin{aligned} u_1(\boldsymbol{x}, t=0) &= \ \ \sin(x_1)\cos(x_2)\cos(x_3) \\ u_2(\boldsymbol{x}, t=0) &= -\cos(x_1)\sin(x_2)\cos(x_3) \\ u_3(\boldsymbol{x}, t=0) &= 0, \end{aligned} \tag{19}$$

and was first considered by Taylor & Green [20] who studied the generation of small-scale turbulence. It is readily apparent from Figs. 2 and 3 that the results are in good agreement with the reference data. Some discrepancies are readily observed, however, these can presumably be attributed to the insufficient spatial resolution. In should emphasized that the results reported in this work were obtained on a 64^3 discrete grid, whereas the reference simulations were carried on a much denser one, i.e. 512^3. For completeness, the author would to like to stress that with increasing spatial resolution, the foregoing differences are significantly reduced (not shown).

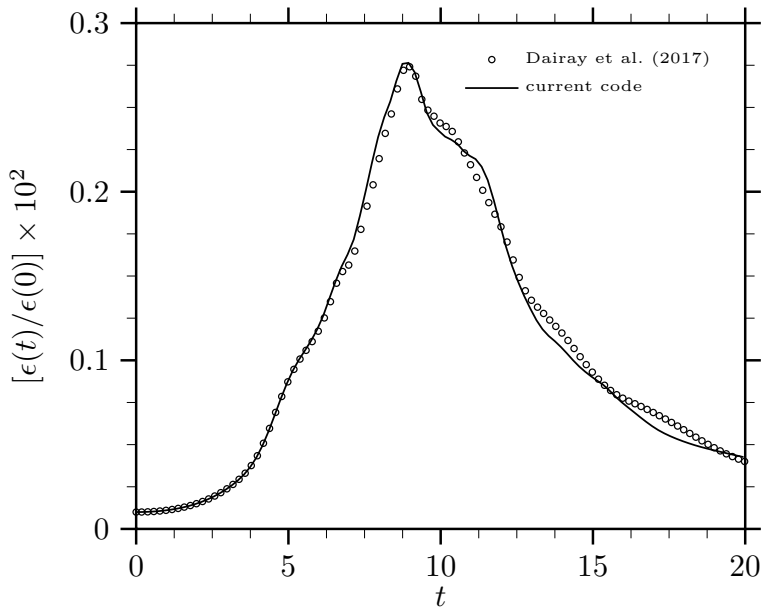

Figure 2: Time history of the normalized energy dissipation at $Re = 1600$. Reference data obtained from [19].

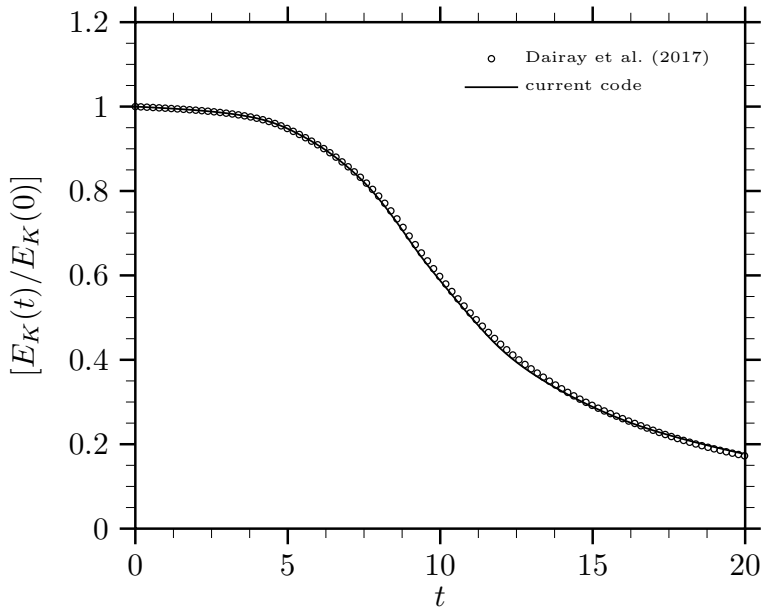

Figure 3: Time history of the normalized energy at $Re = 1600$. Reference data obtained from [19].

6 Lagrangian particle tracking

Consider a small rigid sphere of radius a whose mass is centered at $\boldsymbol{Y}(t)$, which is essentially moving with velocity $V_\alpha(t)$ in an undisturbed velocity field $u_\alpha(\boldsymbol{x}, t)$. If the particle-fluid density ratio is large, say $> 10^3$, than the well-known Maxey & Riley [21] equation of particle motion takes the form of

$$\begin{aligned} \frac{\mathrm{d}V_\alpha}{\mathrm{d}t} &= -f_D \frac{V_\alpha - u_\alpha[\boldsymbol{Y}(t), t]}{\tau_p} + g_\alpha \\ \frac{\mathrm{d}Y_\alpha}{\mathrm{d}t} &= V_\alpha, \end{aligned} \tag{20}$$

where $\tau_p = 2\rho_p a^2/9\mu$ is the particle response time; μ is the dynamic viscosity of the fluid, ρ_p is the particle density; $u_\alpha[\boldsymbol{Y}(t), t]$ denotes the fluid velocity at the particle location, and $\boldsymbol{g}$ is the gravitational acceleration. The non-dimensional correction factor

$$f_D = 1 + 0.15 Re_p^{0.687} \qquad Re_p < 1000 \tag{21}$$

was proposed by Schiller & Neumann [22] to account for the drag force beyond the Stokes flow regime. In the equation above Re_p is the so-called particle Reynolds number defined as

$$Re_p = \frac{\left|\boldsymbol{V} - \boldsymbol{u}\left[\boldsymbol{Y}(t), t\right]\right| d}{\nu}, \tag{22}$$

where d is the particle diameter.

7 Fluid velocity at the particle location

It is readily apparent from Eq. (20) that prior to solving the particle equation of motion, one has to determine the fluid velocity at the particle location. As already indicated, if the velocity field is expanded in the Fourier series, Eq. (6), then the fluid velocity at the instantaneous particle location can be determined by summing the Fourier coefficients. Obviously, the computational cost of this approach can quickly become prohibitively large. In the pseudo-spectral approximation, however, the velocity field is Fourier-transformed to the physical space at each time step, and thus can be relatively easily interpolated to the instantaneous particle locations. For a comprehensive review of various interpolation schemes, one can refer to [23].

Consider an example of a one-dimensional interpolation given in Fig. 4. In this case, the value of an arbitrary function $f(x_p)$ is approximated by

$$f(x_p) \approx \sum_{i=1}^{6} f(x_i) L_i(x_p), \tag{23}$$

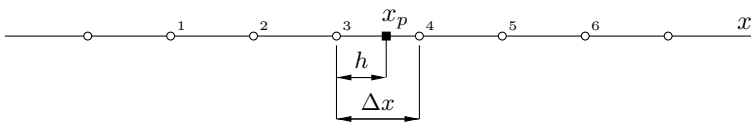

Figure 4: Six-point, one-dimensional Lagrange interpolation; x_p denotes the instantaneous particle location.

where $L_i(x_p)$ are the standard Lagrange basis functions determined at three grid points lying either side of x_p according to

$$L_i(x_p) = \prod_{k=1,k\neq i}^{6} \frac{x_p - x_k}{x_i - x_k}, \tag{24}$$

and thus

$$\begin{aligned} L_1(x_p) &= \frac{x_p - x_2}{x_1 - x_2}\frac{x_p - x_3}{x_1 - x_3}\frac{x_p - x_4}{x_1 - x_4}\frac{x_p - x_5}{x_1 - x_5}\frac{x_p - x_6}{x_1 - x_6} = \\ &= \frac{1}{120}\left(6p - 5p^2 - 5p^3 + 5p^4 - p^5\right), \end{aligned} \tag{25}$$

where $p = h/\Delta x$ with h being the distance between the particle and its closest left neighbor. The full set of basis functions for a one-dimensional Lagrangian interpolation is therefore given by

$$\begin{aligned} L_1(x_p) &= \frac{1}{120}(6p - 5p^2 - 5p^3 + 5p^4 - p^5) \\ L_2(x_p) &= \frac{1}{24}(-12p + 16p^2 - p^3 - 4p^4 + p^5) \\ L_3(x_p) &= \frac{1}{12}(12 - 4p - 15p^2 + 5p^3 + 3p^4 - p^5) \\ L_4(x_p) &= \frac{1}{12}(12p + 8p^2 - 7p^3 - 2p^4 + p^5) \\ L_5(x_p) &= \frac{1}{24}(-6p - p^2 + 7p^3 + p^4 - p^5) \\ L_6(x_p) &= \frac{1}{120}(4p - 5p^3 + p^5) \end{aligned} \tag{26}$$

It can be readily noticed that for a set of N_p particles the foregoing sixth-order Lagrangian interpolation scheme requires $3\times 6^3 \times N_p$ operations to determine the local fluid velocity at the instantaneous particle location, and additionally $3 \times 6^2 \times N_p$ operations to determine the corresponding basis functions.

Using the sixth-order, three-dimensional Lagrangian interpolation scheme, the velocity field at the instantaneous particle location $\boldsymbol{Y}(t) = (x_p, y_p, z_p)$ can be approximated according to

$$u_\alpha(x_p, y_p, z_p) \approx \sum_{i=1}^{6}\sum_{j=1}^{6}\sum_{l=1}^{6} u_\alpha(x_i, y_j, z_l) L_i(x_p) L_j(y_p) L_l(z_p). \tag{27}$$

8 Time integration of the particle equation of motion

In this work, the particle velocity is advanced in time using both the fifth-order implicit Adams-Moulton and the fourth-order explicit Adams-Bashforth schemes essentially leading to

$$V_\alpha^{n+1} = V_\alpha^n - f_D^n\left(\frac{\Delta t'}{720}\Pi_\alpha^{AM} - \frac{\Delta t'}{24}\Pi_\alpha^{AB}\right) \tag{28}$$

where $\Delta t' = \Delta t/\tau_p$, and

$$\begin{aligned} \Pi_\alpha^{AM} &= 251V_\alpha^{n+1} + 646V_\alpha^{n-1} - 264V_\alpha^{n-2} + 106V_\alpha^{n-3} \\ &\quad - 19V_\alpha^{n-4}. \end{aligned} \tag{29}$$

The remaining term on the right-hand side can be determined using

$$\Pi_\alpha^{AB} = 55u_\alpha^n - 59u_\alpha^{n-1} + 37u_\alpha^{n-2} - 9u_\alpha^{n-3}. \tag{30}$$

With the use of Eq. (28), particle trajectories can be advanced in time according to

$$Y_\alpha^{n+1} = Y_\alpha^n + \frac{\Delta t'}{720}\Pi_\alpha^{AM}. \tag{31}$$

9 Conclusions and outlook

In this work, the current stage of development of the pseudo-spectral direct numerical simulations solver intended for studying suspended particle dynamics in homogeneous isotropic turbulence was presented. Preliminary validation indicates that the DNS solver can be considered accurate and reliable. Next steps include the validation of the particulate-phase solver, and the extension of the momentum conservation equation with specific source terms in order to account for the particle-turbulence interaction. In addition to that, the LES solver is to be implemented. However, the last step is rather straightforward and essentially boils down to extending the Navier-Stokes equation, Eq. (14), with the spectral eddy-viscosity ν_e according to

$$\left(\frac{\partial}{\partial t} + \left[\nu + \nu_e(k|k_c)\right] k^2\right) \hat{u}_\alpha = P_{\alpha\beta}\mathcal{F}(\boldsymbol{u}\times\boldsymbol{\omega})_\beta + \hat{f}_\alpha, \tag{32}$$

where, following Chollet & Lesieur [24],

$$\nu_e(k/k_c) = C_K^{-3/2}\left(0.441 + 15.2e^{-3.03k_c/k}\right)\sqrt{\frac{E(k_c)}{k_c}}. \tag{33}$$

In the equation above, C_K is set to 1.4, k_c is a prescribed cutoff wavenumber, and $E(k_c)$ is the kinetic energy density at the cutoff.

Acknowledgments

The work was supported by the National Science Centre (NCN, Poland), research project 2018/30/Q/ST8/00341, and the statutory activities of IMP PAN Gdańsk.

Received in September 2023

References

[1] J. Kuerten, "Point-particle DNS and LES of particle-laden turbulent flow – a state-of-the-art review," *Flow, Turbulence and Combustion*, vol. **97**, pp. 689–713, 2016.

[2] S. Elghobashi, "Direct numerical simulation of turbulent flows laden with droplets or bubbles," *Annual Review of Fluid Mechanics*, vol. **51**, pp. 217–244, 2019.

[3] W. McComb, *The Physics of Fluid Turbulence*. Oxford University Press, Oxford.

[4] O. Reynolds, "On the dynamical theory of incompressible viscous fluids and the determination of the criterion," *Philosophical Transactions of the Royal Society A*, vol. **186**, pp. 123–164, 1894.

[5] D. Leslie, *Developments in the Theory of Turbulence*. Clarendon Press, Oxford, 1990.

[6] S. Orszag, "Numerical methods for the simulation of turbulence," *Physics of Fluids*, vol. **12**, pp. II–250, 1969.

[7] J. Cooley and J. Tukey, "An algorithm for the machine calculation of complex fourier series," *Mathematics of Computation*, vol. **19**, pp. 297–301, 1965.

[8] C. Canuto, M. Hussaini, A. Quarteroni, and T. A. Zang, *Spectral Methods in Fluid Dynamics*. Springer-Verlag, New York, 1987.

[9] G. Patterson Jr and S. Orszag, "Spectral calculations of isotropic turbulence: Efficient removal of aliasing interactions," *Physics of Fluids*, vol. **14**, pp. 2538–2541, 1971.

[10] S. Orszag, "Numerical simulation of incompressible flows within simple boundaries. I. Galerkin (spectral) representations," *Studies in Applied Mathematics*, vol. **50**, pp. 293–327, 1971.

[11] A. Witkowska, D. Juvé, and J. Brasseur, "Numerical study of noise from isotropic turbulence," *Journal of Computational Acoustics*, vol. **5**, pp. 317–336, 1997.

[12] L. Machiels, "Predictability of small-scale motion in isotropic fluid turbulence," *Physical Review Letters*, vol. **79**, p. 3411, 1997.

[13] A. Young, *Investigation of Renormalization Group Methods for the Numerical Simulation of Isotropic Turbulence*. Ph.D. dissertation, University of Edinburgh, 2002.

[14] S. Yoffe, *Investigation of the Transfer and Dissipation of Energy in Isotropic Turbulence*. Ph.D. dissertation, University of Edinburgh, 2012.

[15] V. Eswaran and S. Pope, "An examination of forcing in direct numerical simulations of turbulence," *Computers & Fluids*, vol. **16**, pp. 257–278, 1988.

[16] N. Sullivan, S. Mahalingam, and R. Kerr, "Deterministic forcing of homogeneous, isotropic turbulence," *Physics of Fluids*, vol. **6**, pp. 1612–1614, 1994.

[17] A. Vincent and M. Meneguzzi, "The spatial structure and statistical properties of homogeneous turbulence," *Journal of Fluid Mechanics*, vol. **225**, pp. 1–20, 1991.

[18] L.-P. Wang and M. Maxey, "Settling velocity and concentration distribution of heavy particles in homogeneous isotropic turbulence," *Journal of Fluid Mechanics*, vol. **256**, pp. 27–68, 1993.

[19] T. Dairay, E. Lamballais, S. Laizet, and J. Vassilicos, "Numerical dissipation vs. subgrid-scale modelling for large eddy simulation," *Journal of Computational Physics*, vol. **337**, pp. 252–274, 2017.

[20] G. Taylor and A. Green, "Mechanism of the production of small eddies from large ones," *Proceedings of the Royal Society of London. Series A-Mathematical and Physical Sciences*, vol. **158**, pp. 499–521, 1937.

[21] M. Maxey and J. Riley, "Equation of motion for a small rigid sphere in a nonuniform flow," *Physics of Fluids*, vol. **26**, pp. 883–889, 1983.

[22] L. Schiller and A. Z. Naumann, "Über die grundlegenden berechungen bei der schwerkraftaufbereitun," *Zeitschrift des Vereines Deutscher Ingenieure*, vol. **77**, pp. 318–320, 1933.

[23] S. Balachandar and M. Maxey, "Methods for evaluating fluid velocities in spectral simulations of turbulence," *Journal of Computational Physics*, vol. **83**, pp. 96–125, 1989.

[24] J.-P. Chollet and M. Lesieur, "Parameterization of small scales of three-dimensional isotropic turbulence utilizing spectral closures," *Journal of Atmospheric Sciences*, vol. **38**, pp. 2747–2757, 1981.